Frequency pulling effects in the quasi-two-dimensional ferromagnet ^{54}Mn-Mn$(COOCH_3)_2\cdot 4H_2O$ studied by nuclear orientation techniques

J. Pond, T. Briant, L. Goehring, A. Kotlicki, and B. G. Turrell
Department of Physics and Astronomy, University of British Columbia, Vancouver, British Columbia, Canada V6T 1Z1

C. Itoi
Department of Physics, Nihon University, Kanda, Surugadai, Chiyoda, Tokyo, Japan
(Received 22 March 2001; revised manuscript received 23 April 2001; published 13 July 2001)

Continuous wave NMR thermally detected by nuclear orientation has been used to investigate the magnetic properties and spin dynamics of the quasi-two-dimensional ferromagnet ^{54}Mn-Mn$(COOCH_3)_2\cdot 4H_2O$. The system exhibits a frequency pulling effect due to the indirect Suhl-Nakamura interaction between nuclear spins and the electronic spin excitation spectrum is related to the coupling strength of the nuclear spins. The temperature dependence of the frequency pulling effect was measured for the two crystalline sublattices Mn1 and Mn2 in low magnetic field. The spectra show a structure not predicted theoretically. The current theory is valid only for $I=1/2$ with uniaxial crystalline anisotropy fields. The theory of frequency pulling has been extended here to the case of $I\geqslant 1/2$ and nonuniaxial crystalline anisotropy fields and the resonant frequencies and linewidths have been calculated as a function of temperature. The new theory and data agree well in terms of the magnitude and temperature dependence of the frequency pulling. Discrepancies are likely due to simplifying assumptions when calculating the electronic magnon spectrum. Classical and quantum numerical simulations confirm qualitatively the predictions of the model.

DOI: 10.1103/PhysRevB.64.064403 PACS number(s): 75.40.Gb, 75.10.Jm, 75.30.Ds, 76.60.−k

I. INTRODUCTION

There has been recent interest in the spin dynamics of two-dimensional spin systems[1] and the study of nuclear spin interactions (''frequency pulling'').[2] In a magnetic system, there is a relatively strong coupling between nuclear spins due to the Suhl-Nakamura interaction that involves the virtual emission and reabsorption of an electronic magnon.[3–5] At low enough temperatures, the nuclear spins collectively interact with the electron spins causing a shift in the NMR frequency. Also there are excitations of the nuclear spin system (nuclear magnons). We have chosen to investigate these effects in the quasi-two-dimensional ferromagnet manganese acetate tetrahydrate $Mn(COOCH_3)_2\cdot 4H_2O$ (MnAc), which exhibits relatively large frequency pulling, by studying the abundant ^{55}Mn nuclear spins ($I=5/2$) and very dilute ^{54}Mn radioactive spins ($I=3$) that were doped into the sample during growth. This system has been studied previously by the techniques of nuclear orientation (NO), NMR of Oriented Nuclei (NMRON), and NMR thermally detected by nuclear orientation (NMR-TDNO)[6] and a preliminary measurement of the frequency pulling showed a relatively large effect.

MnAc has a crystallographic layered (a-b) plane structure.[7] The manganese ions in a given layer occupy two different sites (site 1 and site 2) and are arranged in triplet groups consisting of one Mn1 ion and two Mn2 ions which are internally coupled by 120° oxygen and acetate linkages. Each triplet is coupled to four other triplets within a layer by acetate linkages and there are no strong bonds between layers.

The magnetic properties of MnAc have been studied extensively.[7–13] Each Mn^{++} ion has $S=5/2$ and $g\simeq 2.00$.[13,14] Magnetically, the oxygen linkages within a triplet provide a strong superexchange that is antiferromagnetic with an exchange constant $J_{AF,tripl}=48$ K.[9] The superexchange between triplets in a layer is ferromagnetic and much weaker than the intra-triplet antiferromagnetic coupling,[8] and the transition to the ordered state occurs at $T_c=3.19$ K. The interlayer coupling is very weak (~ 1 mK) and antiferromagnetic accounting for the high degree of two dimensionality. The crystal structure and spin orientations of the Mn ions are shown in Fig. 1.

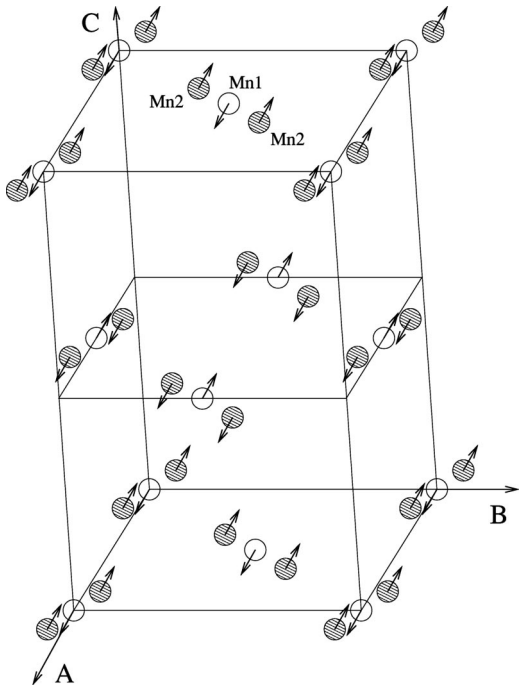

FIG. 1. The MnAc crystal lattice and magnetization. The easy axis of magnetization is the a axis.

The easy axis is the a axis, the second easy axis is the c^* axis (perpendicular to the a-b plane) and the hard direction is the b axis. In order to force the magnetization along the c^* axis (or b axis) it is necessary to apply a field B_A^c (or B_A^b) along the c^* axis (or b axis). These fields are called the anisotropy fields and in MnAc they are $B_A^c = 0.135$ T and $B_A^b = 0.86$ T.[11] At very low temperatures, a field $B_0 = 0.6$ mT applied along the easy axis causes a transition from an antiferromagnetic ordering of the ferromagnetic layers to a mixed phase consisting of domains of ferromagnetic and antiferromagnetic ordering of the planes, and at $B_0 = 14$ mT the planes are completely ordered ferromagnetically.[6]

The strong antiferromagnetic coupling between the spins in a triplet allows us to treat the latter as an effective single spin with $S = 5/2$, ferromagnetically coupled to its neighbors in the ab plane. We also ignore the interlayer interaction and treat the system as purely two dimensional. With these approximations all triplets are equivalent in terms of their magnetic interactions.

A. The ^{54}Mn impurities

The ^{54}Mn impurities have a nuclear spin $I = 3$, a nuclear magnetic moment $\mu = 3.2819 \pm 0.0013 \mu_N$ and decay by electron capture with the subsequent emission of an 835 keV γ ray.[15] A simplified spin Hamiltonian for both the ^{54}Mn1 and ^{54}Mn2 ions in an applied field B_0 is

$$H = H_1 + H_2, \tag{1a}$$

$$H_1 = g\mu_B(B_E \pm B_0)S^z + D\left[S_z^2 - \frac{1}{3}S(S+1)\right], \tag{1b}$$

$$H_2 = A\vec{I}\cdot\vec{S}. \tag{1c}$$

Here H_1 and H_2 represent the electronic and hyperfine interactions, respectively. B_E represents the effective exchange field on a given electronic spin, calculated from mean field theory. The D term represents the crystal field interaction and is related to an anisotropy field by $D = g\mu_B B_A/(2S)$. The term $A\vec{I}\cdot\vec{S}$ represents the hyperfine interaction. The $+$ and $-$ signs are taken for the Mn2 and Mn1 nuclear spins, respectively. We have ignored the electric quadrupole interaction and dipole terms which are very small.[6] This Hamiltonian is clearly oversimplified because we have assumed uniaxial anisotropy.

The H_2 term, representing the hyperfine interaction, can be written as $H_2 = H_{\rm HF} + H'_{\rm HF}$ where $H_{\rm HF} = AS^zI^z$ and $H'_{\rm HF} = A(S^+I^- + S^-I^+)/2$. The effect of $H'_{\rm HF}$ can be treated with perturbation theory.

The zeroth order states of the lowest energy multiplet are characterized by the states $|S^z = -5/2,\ I^z = m\rangle$. The first order correction to the eigenvectors gives a small admixture of the $|S^z = -3/2,\ I^z = m-1\rangle$ states in the lowest energy multiplets. The energy difference between adjacent m and $m+1$ levels in $B_0 = 0$, to second order in $H'_{\rm HF}$ is

$$\Delta E_{m,m+1} = -SA + Pm. \tag{2}$$

Note that the second order effects lead to an unequal splitting of the lowest energy substates. In zero applied field, the ''pseudoquadrupolar'' term P is given by

$$P = \frac{SA^2}{g\mu_B B_E + 4D}. \tag{3}$$

B. The host ^{55}Mn

The abundant ^{55}Mn have a nuclear spin $I = 5/2$ and interact via the Suhl-Nakamura interaction[3,4] that involves the virtual emission of an electronic magnon by one spin and its absorption by another. The Suhl-Nakamura interaction between spins i and j separated by distance r_{ij} can be represented by

$$H_{\rm SN} = \frac{1}{2}\sum_{i,j} U_{ij} I_i^+ I_j^- \tag{4}$$

with

$$U_{ij} = -\frac{A^2 S}{N}\sum_k \frac{\exp(ikr_{ij})}{\omega_k}, \tag{5}$$

where ω_k is the electronic magnon spectrum. In the case of a simple cubic, three-dimensional lattice

$$U_{ij} = \frac{A^2}{g\mu_b B_E}\frac{a}{r_{ij}}\exp\left(-\frac{r_{ij}}{b_0}\right). \tag{6}$$

Here a is the lattice spacing and $b_0 \sim (g\mu_B B_E/E_g)a$ where E_g is the magnon energy gap. Typically the range of the interaction is $b_0 \sim 10a$. Actually, the mechanism for the pseudoquadrupolar interaction for the dilute ^{54}Mn involves the virtual emission/absorption process by a single spin (U_{ii} term).

The Suhl-Nakamura interaction has a number of effects for abundant nuclei. The coupling is usually relatively strong causing fast spin-spin relaxation, i.e., short T_2, and this results in a significant homogeneous line broadening which is usually $\delta\nu_{\rm SN} \geqslant 1$ MHz and dominates other contributions. Furthermore, at very low temperatures ($T \ll 1$ K), when there is a significant nuclear magnetization $\langle I^z\rangle$, the strong Suhl-Nakamura coupling causes the NMR frequency to be pulled down from the value $\nu_0 = AS/h$, to a value $\nu_0 - \Delta\nu$. This effect is called ''frequency pulling.'' Frequency pulling has been discussed, e.g., in Refs. 5,16, and for the special case $I = 1/2$ at very low temperatures

$$\frac{\Delta\nu}{\nu_0} = \frac{A\langle I^z\rangle}{E_g}. \tag{7}$$

There is a band of nuclear magnons, i.e., excitations of the coupled abundant nuclear spins, the spectrum of which covers the range $\nu_0 - \Delta < \nu < \nu_0$. These have been indirectly observed by their effect of enhancing the nuclear spin-lattice relaxation (NSLR) of the ^{54}Mn2 compared to ^{54}Mn1 because the frequency of the former is closer to the nuclear magnon band, and directly observed by NMR.[6] Values of $(\Delta\nu/\nu_0)$ (Mn1) $= 0.05$ and $(\Delta\nu/\nu_0)$ (Mn2) $= 0.06$ were ob-

served at $T \sim 40$ mK. The expected values of 0.09 and 0.10 for the Mn1 and Mn2 spins, respectively, calculated from Eq. (7), were significantly different from the measured values. It was noted that these effects would be investigated further, and this is the purpose of the present study.

C. The effect of the Suhl-Nakamura interaction on the ^{54}Mn impurities

The dilute ^{54}Mn spins are also coupled to their neighbors via the Suhl-Nakamura interaction. The effect of this interaction on the energy levels of the lowest order multiplet can be calculated using nondegenerate perturbation theory because the ^{54}Mn are sufficiently dilute that we can treat them as a single impurity (at $\vec{R}=0$) in a lattice of ^{55}Mn spins.

The first order correction to the energy is simply another way of calculating the pseudoquadrupolar interaction, and gives the same result as Eq. (2). The second order corrections can be shown to be negligible compared to the first order correction, therefore, the only significant effect of the Suhl-Nakamura interaction on the ^{54}Mn spins is the self-interaction (or pseudoquadrupolar term), as discussed in Sec. I A.

II. EXPERIMENTAL PROCEDURE

A. Sample preparation and data acquisition

Seed crystals of approximately 1 mm in length were grown from a saturated solution of MnAc by evaporation at room temperature. To prevent oxidation, a seed crystal was placed in a groove cut in a piece of teflon, approximately 5 mm in width, and oriented according to the goniometric data of Groth.[19] The groove was covered with a microscope slide and sealed to the Teflon with vacuum grease. Saturated MnAc solution was prepared and doped with approximately 100 μCi of ^{54}Mn. Once the saturated solution surrounded the seed crystal, the temperature of the bath was lowered slowly over a period of 4 days from 30 to 23 °C. The final crystal had the orientation of the seed crystal, and an activity of approximately 1 μCi. The orientation of the crystal was verified by x-ray diffraction. The crystal was attached to the copper cold finger of a SHE dilution refrigerator with the easy axis (a axis) aligned vertically. Hydrated crystals deteriorate at reduced pressure at $T \geqslant 240$ K so the samples were precooled under an atmosphere of air.

In order to study the spin dynamics we employ two techniques that combine nuclear orientation (NO) with NMR. Nuclear spins can be oriented at sufficiently low temperatures when acted on by a magnetic field. In the case of MnAc, the hyperfine interaction gives the largest contribution to the applied field, and significant orientation is achieved when $T \leqslant A/k_B$.

The directional anisotropy of the 835 keV γ ray emitted in the decay of the ^{54}Mn can be used to measure the degree of orientation of the initial ensemble of nuclei. The angular distribution of γ rays at 0° and 90° to the easy axis $W(0)$ and $W(90)$, can be expressed as[17]

$$W(0) = \frac{5}{3}(p_2 + p_{-2}) + \frac{4}{3}(p_1 + p_{-1}) + p_0, \tag{8a}$$

$$W(90) = \frac{5}{4}(p_3 + p_{-3}) + \frac{5}{4}(p_2 + p_{-2}) + \frac{3}{4}(p_1 + p_{-1}) + \frac{1}{2}p_0, \tag{8b}$$

where $m = I^z$ and p_m are the level populations, given to a good approximation by

$$p_m \simeq \frac{\exp\left(\frac{SAm}{k_B T}\right)}{\sum_m \exp\left(\frac{SAm}{k_B T}\right)}. \tag{9}$$

Having achieved a significant γ-ray anisotropy by cooling the sample to a low temperature, NMR of Oriented Nuclei (NMRON) can be performed by applying a radiofrequency (rf) field and sweeping the frequency. When the rf field is at a resonance of the ^{54}Mn spins the level populations p_m are altered and there is a resulting change in $W(0)$ and $W(90)$. This allows a direct measurement of the hyperfine coupling constant, A. For the dilute ^{54}Mn spins, the resonant frequencies $\nu_{m,m+1} = \Delta E_{m,m+1}/h$ corresponding to $m \rightarrow m+1$ transitions, can be selectively observed. The ^{54}Mn spins were investigated by NMRON and, using Eq. (2), gave $\langle {}^{54}AS \rangle_1 / h = 437.0 \pm 0.2$ MHz for the Mn1 site, $\langle {}^{54}AS \rangle_2 / h = 480.5 \pm 0.2$ MHz for the Mn2 site, and $P/h = 1.2 \pm 0.1$ MHz.[6]

If the hyperfine coupling constant is known, as it is from the NMRON measurements, then the γ-ray anisotropy allows the temperature of the crystal to be determined, i.e., $W(\theta)$ is a thermometer. If NMR is performed on the stable, abundant ^{55}Mn spins, the effect of the absorbed power is to increase the temperature of the lattice via the spin-lattice relaxation. The increased temperature affects the level populations of the ^{54}Mn and can be observed by a change in $W(\theta)$. Thus, the nuclear orientation of the ^{54}Mn is the thermometric probe which measures the increase in temperature of the sample due to the NMR resonance of the host, ^{55}Mn spins. This technique is called NMR thermally detected by nuclear orientation (NMR-TDNO).[18]

The beauty of combining NMRON and NMR-TDNO is that the effects of the Suhl-Nakamura interaction can be observed directly by comparing the NMR signals of the abundant ^{55}Mn spins, that feel the interaction, and the ^{54}Mn that do not. In a 1 cm^3 crystal of ^{54}Mn-$MnCl_2 \cdot 4H_2O$ with 5 μCi activity, the separation of the ^{54}Mn atoms is $\sim 1000a$ which is much larger than the range of the interaction. The linewidth is only ~ 35 kHz because there is no broadening from the Suhl-Nakamura interaction, whereas the linewidth of the ^{55}Mn resonance is several MHz and there is frequency pulling. The NMRON results on ^{54}Mn allows the hyperfine field of ^{55}Mn to be determined so that the value of the unpulled frequency ν_0 is known.

In order for NMR-TDNO to work well, the spin-lattice relaxation time T_1 should be short compared to the dwell time of the rf frequency step and the time constant for the

cooling of the sample to the cold finger. In zero field, the spin lattice relaxation times are $\sim 10^{-1}$ s,[6] and the γ-ray anisotropy of the ^{54}Mn spins provides an accurate measure of the temperature of the ^{55}Mn spins. The isotropic warm counts necessary to normalize the counting rates were obtained at $T \sim 1$ K. The spectra were obtained with two NaI detectors at 0° and 90° to the easy axis.

In the previous experiment,[6] only one measurement of the ^{55}Mn lines was made, and no structure was observed. Also, no measurements were performed above 600 MHz. The rf power was stabilized by monitoring the temperature of the cold finger, but this has two disadvantages: first, the time constant of the feed-back loop was relatively long; secondly, the cold finger must undergo some warming at resonance, but the feed-back loop works to negate the effect. This stabilization procedure works well for NMRON of the dilute radioactive nuclei because there is essentially no warming, but is not well suited to the NMR-TDNO technique.

In the present experiment, the rf field was provided by a main coil in series with a variable capacitor and in parallel with a fixed capacitor. The circuit had a broad resonance centered approximately at 530 MHz at 100 mK. The rf power was monitored by a smaller pickup coil mounted behind the main coil. This pickup coil had no resonances in the frequency region of interest. The signal from the pickup coil was amplified and converted to dc with a Pasternack 8000-50 detector connected to an HP voltmeter, read by a PC. The PC continually adjusted the rf power to maintain a constant signal in the pickup coil. This feedback loop allowed the rf power to be stabilized over the entire range of the frequency sweeps (>100 MHz). This arrangement eliminated the effects of frequency-dependent rf heating of the cold finger. This improved detection method allowed the resolution of the structure of the lines. Several spectra were obtained corresponding to different ^{55}Mn nuclear spin temperatures and these showed four peaks rather than the expected two.

In the thermometric method of detecting the resonances, sweeps upward and downward in frequency yield different line shapes due to the frequency pulling effect itself. The resonance is detected by a warming of the crystal lattice but this also leads to an upward shift the resonant frequency. Thus downward frequency sweeps lead to a narrowing of the observed lines while upward sweeps lead to a broadening. The most precise determination of the resonant frequencies can therefore be made with downward frequency sweeps. Figure 2 shows three spectra at different temperatures in zero applied field for a downward frequency sweep and the frequency pulling effect can be clearly observed. The same spectra were observed in applied fields up to 110 mT along the easy axis.

B. Data analysis

In order to estimate the line positions as a function of temperature, the peaks were fitted by assuming a Gaussian line shape and an exponential relaxation to the temperature of the dilution refrigerator. The change in anisotropy at frequency ω is then given by

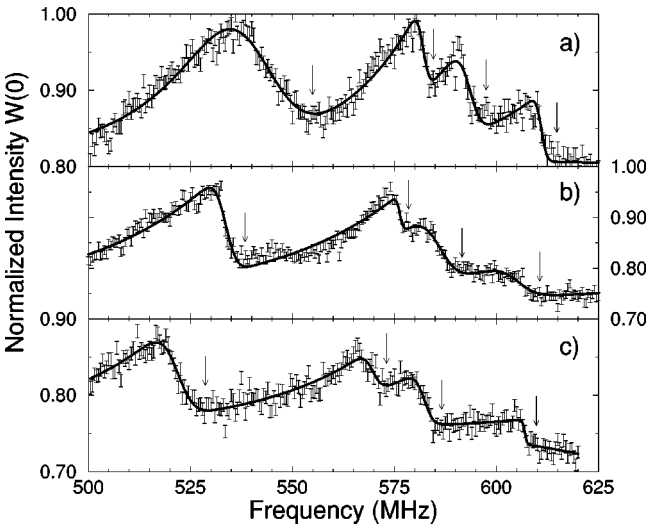

FIG. 2. $W(0)$ as a function of frequency for three spectra with the best fit line. Although the temperature of the sample varies throughout the frequency sweep (from about 30 mK to over 100 mK), in general $T_a > T_b > T_c$ and the frequency pulling can be clearly seen. The initial temperatures for each of the three sweeps is $T_a = 41$ mK, $T_b = 34$ mK, and $T_c = 32$ mK. The frequency was swept downwards, and the region of points where the temperature was determined for each of the resonant lines is labeled with an arrow.

$$\frac{dW(0)}{dt} = \sum_{i=1}^{4} A_i \int_{-\phi_0}^{\phi_0} \exp\left(\frac{-(\omega + \phi - \omega_i)^2}{\sigma_i^2} \right) d\phi + \frac{W_0(0) - W(0)}{\tau}, \tag{10}$$

where the first term corresponds to the four NMR resonances, and the second term is the relaxation to the base anisotropy $W_0(0)$. ϕ_0 is the modulation of the rf field, τ is the relaxation time, and A_i, ω_i, and σ_i are the amplitudes, positions, and widths of the four resonances. The starting anisotropy was taken to be the average of the first five data points. $W(0)$ was then calculated by integrating Eq. (10) with respect to t and a χ^2 was calculated and minimized with MINUIT. $W_0(0)$ was not necessarily equal to the starting anisotropy because turning on the rf power did affect the base temperature of the crystal through nonresonant warming of the cold finger. An example of a fit can be seen in Fig. 2.

Five experimental points $W(0)$ were averaged immediately prior to each observed resonance and the temperature was then determined from Eq. (8b). The points at which the temperatures were determined are labeled in Fig. 2 with arrows. Although the relaxation processes and the power absorption are more complicated than the assumptions of the model, the goal was to find the position of the NMR lines as a function of temperature and this is clearly achieved. The width of the lines (σ_i) are used as the error in line position. The position of the lines as a function of temperature are plotted in Fig. 3. In order to fit the data exactly, a theoretical model of the entire power spectrum as a function of temperature would be necessary. However, the Gaussian fit gives a

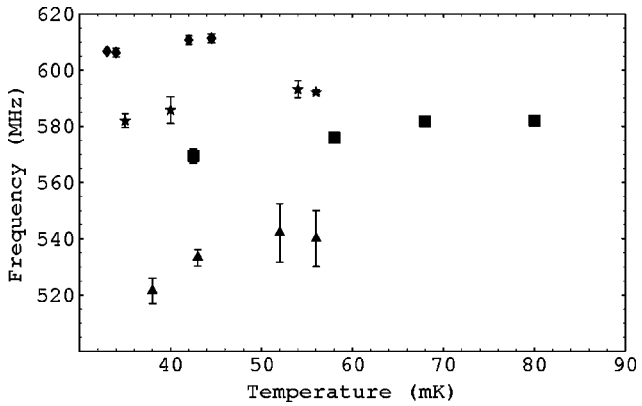

FIG. 3. The positions of each of the four resonant lines at different temperatures.

very reasonable estimate, within the given error, of the position of the lines as a function of temperature.

III. THE GENERAL SUHL-NAKAMURA INTERACTION: A BASIS OF SPINS, $I \geqslant 1/2$ AND NONUNIAXIAL ANISOTROPY

The simple model of the Suhl-Nakamura interaction for the case $I=1/2$ with uniaxial anisotropy and a single ion per lattice site, as outlined in Sec. I, is clearly insufficient to explain the observed spectra. To the best knowledge of the authors, the Suhl-Nakamura interaction with $I>1/2$ has not been previously considered. When $I>1/2$ the self-interaction term (U_{ii}) cannot be neglected. Also, when there is nonuniaxial anisotropy, the electronic magnon gap which determines the overall amplitude of the frequency pulling needs to be calculated by a Bogliubov transformation. Finally, when there is a triplet of ions at each lattice site, the interactions between the Mn1 and Mn2 spins cannot be ignored and will modify the frequency pulling. We have developed a model which takes all of these important effects into account.

In the following section, the frequency pulling is calculated for a triplet of spins and compared to the experimental data. Furthermore, the $T=0$ spectrum of excitations calculated by spin wave theory is discussed. The effects of the Mn1 spins on Mn2 spins and vice versa is found to be important. A number of mechanisms which could explain the four observed lines are considered.

The linewidth is calculated in the case of a single spin per lattice site down to $T=0$ and compared to a high-temperature expansion previously calculated. The results agree well at the temperatures where the high-temperature expansion is valid. However, our calculation also includes the effects of the self-interaction on the linewidth, and is valid as $T \rightarrow 0$.

The exact power spectrum involving 1 to 4 spins is calculated numerically at a variety of temperatures and classical simulations are performed. The results qualitatively confirm the predictions of our model.

A. The electronic magnon spectrum

The strong coupling between the three electronic spins forming a triplet allows us to treat the latter as an effective $S=5/2$ single spin, ferromagnetically coupled to its neighbors in the a-b plane. We can also ignore the magnetic interactions between different layers and treat the system as a 2D ferromagnet. The z direction is chosen along the a axis, and the x and y directions are chosen to be the b and c^* axes, respectively.

The electronic magnon gap can be calculated from the electronic spin Hamiltonian

$$H = J_F \sum_{\langle nn \rangle} \vec{S}_i \cdot \vec{S}_j + \sum_i g\mu_B \left(\frac{B_A^b}{2S} (S_i^x)^2 + \frac{B_A^c}{2S} (S_i^y)^2 - S_i^z B_0 \right). \tag{11}$$

A standard Holstein-Primakoff transformation can be used, in which $S^z = S - a^\dagger a$, $S^+ \simeq \sqrt{2S}a$, and $S^- \simeq \sqrt{2S}a^\dagger$. This transformation is expected to give good results because the spin is large ($S=5/2$) and the temperature is low compared to the coupling between electronic spins ($T < 100$ mK whereas $T_c \sim 3$ K). It is then more convenient to work in momentum space.

The Hamiltonian is not diagonal because the anisotropy fields in the b and c directions are different, and it is necessary to perform a Bogliubov transformation. (For a complete discussion of diagonalization of bosonic and fermionic annihilation and creation operator Hamiltonians, see Ref. 20.) New fields, α_k and $\alpha_{-k}^\dagger$, can be introduced and are defined as

$$\begin{pmatrix} \alpha_k \\ \alpha_{-k}^\dagger \end{pmatrix} = \begin{pmatrix} u_k & -v_k \\ -v_k & u_k \end{pmatrix} \begin{pmatrix} a_k \\ a_{-k}^\dagger \end{pmatrix}. \tag{12}$$

The Hamiltonian is $H - E_0 = \Sigma_k \omega_k \alpha_k^\dagger \alpha_k$ for a suitable choice of u_k and v_k, where E_0 is the ground state energy. It is important to note that u_k is significantly different from unity, and v_k from zero, only near $k=0$. If the anisotropy fields are uniaxial ($B_A^c = B_A^b$) then $u_k = 1$ and $v_k = 0$. The electronic magnon spectrum is given by

$$\omega_k = \sqrt{\Omega_0^2(k) - (g\mu_B B_A^-)^2}, \tag{13}$$

where $B_A^- = (B_A^b - B_A^c)/2$ and $\Omega_0^2(k)$ is the electronic magnon spectrum calculated in the case of uniaxial anisotropy fields with $B_A = (B_A^c + B_A^b)/2$. The electronic magnon gap is $\omega_0 / g\mu_B = 0.35$ T, for $B_A^b = 0.14$ T and $B_A^c = 0.86$ T.[11] For these values of B_A^b and B_A^c, $u_k = 1.105$ and $v_k = -0.470$ when $k \rightarrow 0$.

B. The Suhl-Nakamura interaction between nuclear spins

The Suhl-Nakamura interaction can be calculated for the MnAc crystal, with the assumption that the electronic spins in a triplet behave as a single, $S=5/2$ spin coupled to each of the three nuclear spins. If we introduce the operator

$$\vec{\Lambda}_j = \mathbf{A_1} \vec{I}_j + \mathbf{A_2} (\vec{I}_{a,j} + \vec{I}_{b,j}), \tag{14}$$

where $\mathbf{A_1}$ and $\mathbf{A_2}$ are the effective hyperfine coupling tensors of the sites 1 and 2 and the indices a and b refer to the two equivalent Mn2 sites, then the hyperfine Hamiltonian can be expressed as

$$H_{\mathrm{HF}}=\sum_j \vec{\Lambda}_j\cdot\vec{S}=\sum_j\left(\Lambda_j^z S_j^z+\frac{1}{2}(\Lambda_j^+ S_j^-+\Lambda_j^- S_j^+)\right), \tag{15}$$

where $\Lambda_j^{\pm}=\Lambda_j^x\pm i\Lambda_j^y$.

Working in momentum space and using the Holstein-Primakoff transformation, introduced above, the electronic spins can be rewritten in terms of a_k and $a_{-k}^{\dagger}$. Finally, the hyperfine Hamiltonian can be written in terms of the operators α_k and $\alpha_{-k}^{\dagger}$, defined in Eq. (12). The Hamiltonian is $H=H_0+H'$ where

$$H_0=S\sum_j \Lambda_j^z+\sum_k \omega_k\alpha_k^{\dagger}\alpha_k, \tag{16}$$

and H' is a function of u_k, v_k, and $\alpha_k^{\dagger}$. If we consider H' as a perturbation of H_0, we can calculate the correction to the energy for a state $|\Psi\rangle=|\psi_0\phi\rangle$, where $|\psi_{n,k_1,\ldots,k_n}\rangle$ is the electronic state with n magnons of wave vector $k_1,\ldots,k_n$, and $|\phi\rangle$ is an arbitrary nuclear state. There is no first order correction to the energy and, to second order, only terms with one or two electronic magnons contribute. Using the fact that $\omega_k\gg\Delta E_{\psi}$, the second order corrections to the energy can be shown to be equivalent to the diagonal matrix elements of an effective nuclear Hamiltonian

$$H_{eff}=\frac{1}{2}\sum_{j,j'}[U_{jj'}^{++}(\Lambda_j^-\Lambda_{j'}^-+\Lambda_j^+\Lambda_{j'}^+)+U_{jj'}^{+-}\Lambda_j^+\Lambda_{j'}^- +U_{jj'}^{-+}\Lambda_j^-\Lambda_{j'}^++2U_{jj'}^z\Lambda_j^z\Lambda_{j'}^z] \tag{17}$$

with

$$U_{jj'}^{++}=-\frac{S}{N}\sum_k\frac{u_k v_k e^{ik(R_j-R_{j'})}}{\omega_k}, \tag{18a}$$

$$U_{jj'}^{+-}=-\frac{S}{N}\sum_k\frac{u_k^2 e^{ik(R_j-R_{j'})}}{\omega_k}, \tag{18b}$$

$$U_{jj'}^{-+}=-\frac{S}{N}\sum_k\frac{v_k^2 e^{ik(R_j-R_{j'})}}{\omega_k}, \tag{18c}$$

$$U_{jj'}^{z}=-\frac{1}{N^2}\sum_{k_1,k_2}\frac{(u_{k_1}v_{k_2}+u_{k_2}v_{k_1})^2 e^{-i(k_1+k_2)(R_j-R_{j'})}}{\omega_{k_1}+\omega_{k_2}}. \tag{18d}$$

C. The pseudoquadrupolar interaction

We consider first the pseudoquadrupolar interaction for ^{54}Mn. In this case, there is no coupling between nuclear spins because they are so dilute. It is clear that $U_{ii}^{+-}\gg U_{ii}^{-+}$, $U_{ii}^{+-}\gg U_{ii}^{++}$ and $U_{ii}^{+-}\gg U_{ii}^{z}$ because $u_k\gg v_k$ except for a small region near $k=0$. This conclusion is supported by numerical results. Consequently, we shall ignore all terms except those involving U_{ii}^{+-}.

Using $I^+I^-=I(I+1)-(I^z)^2+I^z$, and assuming an isotropic hyperfine interaction A, the Hamiltonian for each spin (1 or 2) reduces to

$$H=ASI^z+\frac{A^2}{2}[I(I+1)-(I^z)^2+I^z]U_{ii}^{+-} \tag{19}$$

and the difference in energy between levels m and $m+1$ is given by

$$h\nu_{m,m+1}=AS-mA^2U_{ii}^{+-}. \tag{20}$$

We can compare to values measured for ^{54}Mn[6] where, in $B_0=0.2$ T, the value of $-(A_2^{54})^2U_{ii}^{+-}/h$ for the Mn2 site is found to be 1.2 MHz. The mean field Curie temperature for a Heisenberg Hamiltonian is given by[21]

$$k_BT_c^{mf}=\frac{4}{3}S(S+1)J. \tag{21}$$

Our magnetic system is a Hamiltonian with nearest neighbor coupling (equivalent to a square lattice model since J is the same for all 4 nearest neighbors). From the exact two-dimensional square lattice result for an Ising, nearest neighbor model, we know that $T_c/T_c^{mf}=0.567$.[22] Since $T_c=3.19$ K for MnAc, we can predict that $J/k_B\simeq 0.456$ K. Using $B_A^c=0.14$ T, $B_A^b=0.86$ T, $B_0=0.2$ T, and $J/k_B=0.456$ K, we find that $-(A_2^{54})^2U_{ii}^{+-}=1.1$ MHz, which compares very well with the experimental result of 1.2 MHz.

D. The interaction for the host spins

In the case of the abundant ^{55}Mn spins, the interaction between neighboring spins cannot be ignored. The six equations of motion for $I_{\alpha,j}^{\pm}$, where α denotes the Mn1 or Mn2 site ($\alpha=1,2$), are given by

$$\frac{dI_{\alpha,j}^{\pm}}{dt}=i[H,I_{\alpha,j}^{\pm}]. \tag{22}$$

We can linearize these equations by replacing $I_{\alpha,j}^z$ with its thermodynamic average $\langle I_{\alpha}^z\rangle$. This approximation leaves an indeterminacy in the equations because $\langle I_{\alpha}^z\rangle$ is a c number and the commutation relations with $I_{\alpha,j}^{\pm}$ are lost. However, it can be shown that the terms due to the commutation relations either lead to a small renormalization of the unpulled frequency or are small enough to be neglected. If we work in momentum space, the linearized equations of motions can be written in the following form:

$$-i\frac{d}{dt}\begin{pmatrix} I_k^+\\ I_{a,k}^+\\ I_{b,k}^+\\ I_{-k}^-\\ I_{a,-k}^-\\ I_{b,-k}^-\end{pmatrix}=G_k(T)\begin{pmatrix} I_k^+\\ I_{a,k}^+\\ I_{b,k}^+\\ I_{-k}^-\\ I_{a,-k}^-\\ I_{b,-k}^-\end{pmatrix}, \tag{23}$$

where the indices a and b refer to each of the two Mn2 sites, and the elements of $G_k(T)$ depend on the hyperfine coupling constants, the values of u_k and v_k and the thermodynamic averages $\langle I_1^z\rangle$ and $\langle I_2^z\rangle$.

Finally, the power spectrum can be calculated from

$$P(\omega,k)=\int dt e^{i\omega t}[\langle \Upsilon_k^-(t)\Upsilon_k^+(0)\rangle+\langle \Upsilon_k^+(t)\Upsilon_k^-(0)\rangle], \tag{24}$$

where $\Upsilon=I_k^{\pm}(t)+I_{a,k}^{\pm}(t)+I_{b,k}^{\pm}(t)$. The resonant lines in the NMR power spectrum will correspond to the eigenvalues of the matrix $G_{k=0}(T)$. There are three excitation modes. The first corresponds to an optical mode where the two Mn2 sites precess in opposition of phase and there is no precession of the Mn1 spins. This optical mode has no frequency pulling, and is at the unpulled frequency of the Mn2 spins. From Eq. (24) it is clear that this mode should not be absorbed. Indeed, there is no net precession of the magnetization and this mode should not couple to the precessing magnetic field.[23] The other two modes involve precession of all three spins, but the Mn2 precess exactly in phase. Also, the higher frequency mode corresponds almost entirely to precession of the Mn2 spins, while the lower frequency mode corresponds mostly to motion of the Mn1 spin. This admixture between Mn1 and Mn2 spins decreases with increasing separation of the unpulled frequencies. Both of these modes are frequency pulled, and the resonant frequencies decrease with decreasing temperature.

E. The frequency pulling at $T=0$ calculated with spin wave theory

The low-temperature limit of the theory can be calculated using spin wave theory. The details are similar to the calculation of the electronic magnon spectrum in spin wave theory. The nuclear Hamiltonian can be expressed as annihilation and creation operators of nuclear magnons by a Holstein-Primakoff transformation. The Hamiltonian can then be diagonalized by performing a Boguliubov transformation of six fields. This can be solved as a simple eigenvalue problem by diagonalizing in the correct metric (see Ref. 20). Practically, the eigenvalue and eigenvectors involve diagonalizing a matrix which is equal to $G_k(T=0)$. Thus the spectrum calculated by spin wave theory gives precisely the $T=0$ result calculated previously.

F. Linewidth

The calculation of the second moment is quite complicated because three spins are involved. Therefore, the case of a single spin with uniaxial anisotropy, but arbitrary I, will be considered in order to understand the behavior of the linewidth as a function of temperature. To the best knowledge of the authors, the linewidth has not been previously calculated with $I>1/2$ or as $T\rightarrow 0$.

The Suhl-Nakamura Hamiltonian in this case is

$$H=H_0+H_1=AS\sum_i I_i^z+\frac{1}{2}\sum_{ij} U_{ij}I_i^+I_j^-. \tag{25}$$

The power spectrum is given by

$$P_k(\omega)=\int dt\langle I_k^+(t)I_k^-(0)\rangle\exp(i\omega t). \tag{26}$$

Because $AS\gg\Sigma_i U_{ij}$ we can, to an excellent approximation, calculate the thermodynamic averages with $H=H_0$. Following Van Vleck's method of moments,[24] we can calculate the first and second moments of the power spectrum and the width of the resonance $(\Delta\omega)^2=\langle\omega^2\rangle-\langle\omega\rangle^2$ can then be calculated.

Since we are interested in the uniform mode $(k=0)$, only that case will be considered. When calculating the thermodynamic averages, we have used $H=H_0$ and therefore $\langle I_i^+I_m^zI_j^-\rangle=\langle I_i^+I_j^-\rangle\langle I_m^z\rangle\delta_{ij}$ when $i\neq m$. Of course, when $i=m$ we can, to a good approximation at low temperatures, use $\langle I_i^+I_m^zI_j^-\rangle=\langle I_i^+I_j^-\rangle\langle I_m^z-1\rangle\delta_{ij}$. With these approximations, the first moment gives the same result as Eq. (7).

The second moment has been calculated using an expansion in $1/T$ by Pincus,[25] and the linewidth is found to be

$$(\Delta\omega)=(\Delta\omega_\infty)\left(1-\frac{3|\delta\omega|}{8\langle\omega\rangle}\right), \tag{27}$$

where $(\Delta\omega_\infty)$ is the high-temperature linewidth and $\delta\omega=\Sigma_i U_{im}\langle I^z\rangle$ is the frequency pulling. However, this result has two problems for our application. First, it is only valid when $AS\ll k_BT$ which is certainly not the case at the temperatures obtained in our experiments. Secondly, it is calculated assuming that there is no self interaction term $(U_{ii}=0)$.

The second moment can be calculated, in the general case, by using $H=H_0$ to evaluate thermodynamic averages and by assuming that

$$\langle I_i^+I_i^zI_i^-\rangle\sim\langle I_i^+I_i^-\rangle\langle I_i^z-1\rangle, \tag{28a}$$

$$\langle I_i^+I_i^zI_i^zI_i^-\rangle\sim\langle I_i^+I_i^-\rangle\langle(I_i^z-1)^2\rangle. \tag{28b}$$

The final result for the linewidth is

$$\begin{aligned}(\Delta\omega)^2=U_{ii}\left(\sum_i U_{ij}\right)\left[\frac{3\langle(I^z)^2\rangle}{2}+\frac{|\langle I^z\rangle|}{2}-\frac{I(I+1)}{2}-\langle I^z\rangle^2\right]\\+\sum_i U_{ij}^2\left[\langle I^z\rangle^2-\frac{|\langle I^z\rangle|}{2}+\frac{I(I+1)}{2}-\frac{\langle(I^z)^2\rangle}{2}\right]\\-U_{ii}^2\langle I^z\rangle^2.\end{aligned} \tag{29}$$

Note that, at high temperature $\langle I^z\rangle=0$ and $\langle(I^z)^2\rangle=I(I+1)/3$. Therefore $(\Delta\omega_\infty)^2=\frac{1}{3}\Sigma_i U_{ij}^2I(I+1)$. This is precisely the result of Van Vleck[24] calculated at the high-temperature limit and is also the high-temperature limit used by Pincus.[25] Since the result of Pincus is only valid for $U_{ii}=0$, we can compare the two predictions in this case (see Fig. 4). The results agree well when $k_BT\gg AS$ when the high temperature expansion is valid, but they deviate markedly at low temperatures when our approximation should be valid.

It is also useful to consider the case where only the self-interaction term is present. In this case

$$(\Delta\omega)^2=U_{ii}^2[\langle(I^z)^2\rangle-\langle I^z\rangle^2]. \tag{30}$$

This is exactly the result expected for a pseudoquadrupolar splitting. At $T=0$ only the lowest energy level is occupied

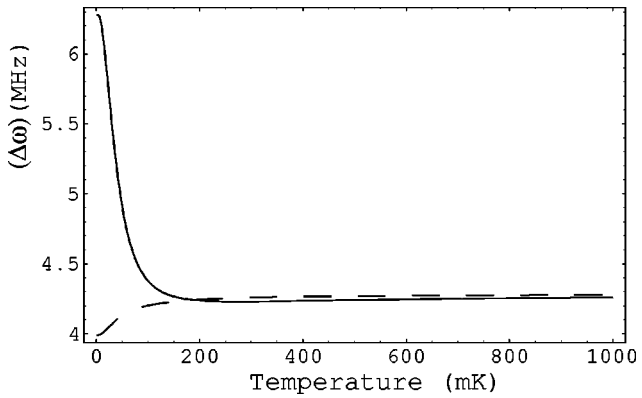

FIG. 4. The mean square width for $U_{ii}=0$, $\Sigma_i U_{ij}/h = 14.1$ MHz, and $\Sigma_i U_{ij}^2/h^2 = 6.3$ MHz^2. The dashed line is the prediction of Pincus.

and the line is infinitely narrow. At $T=\infty$, the resonance is made up of six individual transitions of equal amplitude, with a spacing U_{ii} between each. The linewidth for such a resonance is clearly on the order of $U_{ii}I$.

The result when U_{ii} is not zero is shown in Fig. 5. The temperature dependence of the linewidth is very surprising and the sharp minimum falls in the range of temperatures used in our experiments. Some of the unusual temperature dependence of the linewidths in the experimental data may indicate that these effects are present. Unfortunately, the second moment has not been calculated in the case of the triplet nuclear spins because it is difficult to find which terms contribute to which of the four lines. In order for a second moment calculation to be meaningful only terms contributing to a single resonant line should be included.

G. Numerical simulations

In order to explore the possibility that the splitting of the pulled Mn2 line could be lost in the linearization procedure or is due to an enhanced pseudoquadrupolar splitting, we have calculated numerically the exact power spectrum for up to four spins with $I=5/2$, including nearest neighbor interactions. The simplified Hamiltonian used, for a single spin has the form

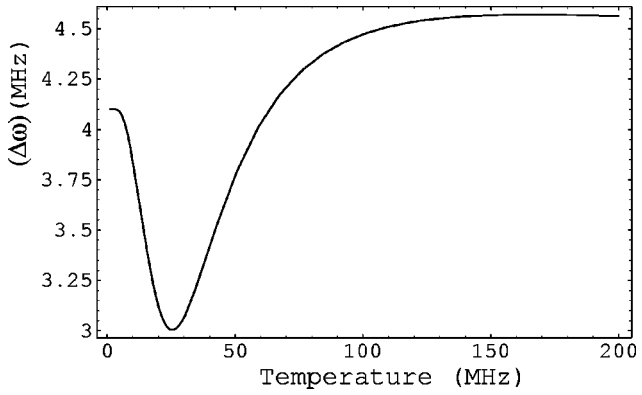

FIG. 5. The mean square width for $U_{ii}/h=1.9$ MHz, $\Sigma_i U_{ij}/h=14.1$ MHz, and $\Sigma_i U_{ij}^2/h^2=6.3$ MHz^2.

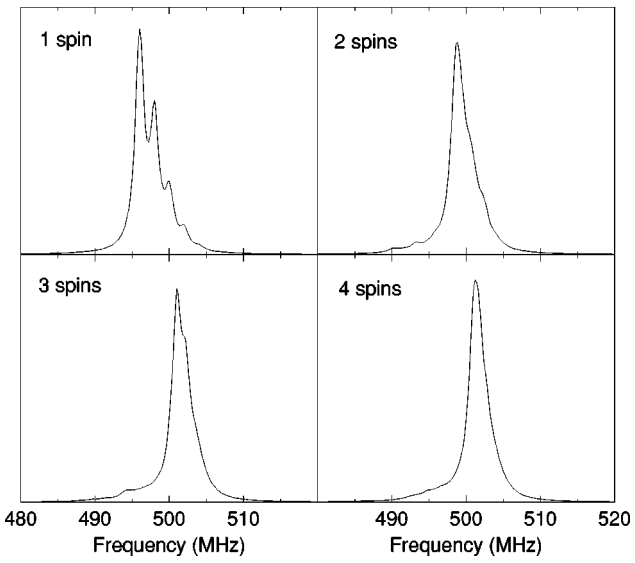

FIG. 6. The exact power spectrum for one to four spins at $k_B T/h = 500$ MHz or $T=24$ mK, including pseudoquadrupolar interactions of 2 MHz and nearest neighbor interactions of 1 MHz

$$H=\sum_i \left(aI_i^z + \frac{b}{2} I_i^+ I_i^- \right) + \frac{c}{2} \sum_{\langle ij \rangle} I_i^+ I_j^- , \qquad (31)$$

where $\langle ij \rangle$ denotes a sum over nearest neighbors. In the simulations, $a/h=500$ MHz, $b/h=2$ MHz, and $c/h = 1$ MHz. The power spectrum is calculated by diagonalizing the Hamiltonian and using Eq. (26). The results for one to four spins at $k_B T/h=500$ MHz can be seen in Fig. 6, and for four spins at different temperatures in Fig. 7. These numerical results indicate that the pseudoquadrupolar structure is smoothed out as the number of interacting spins increases, and is likely not responsible for the observed structure. The

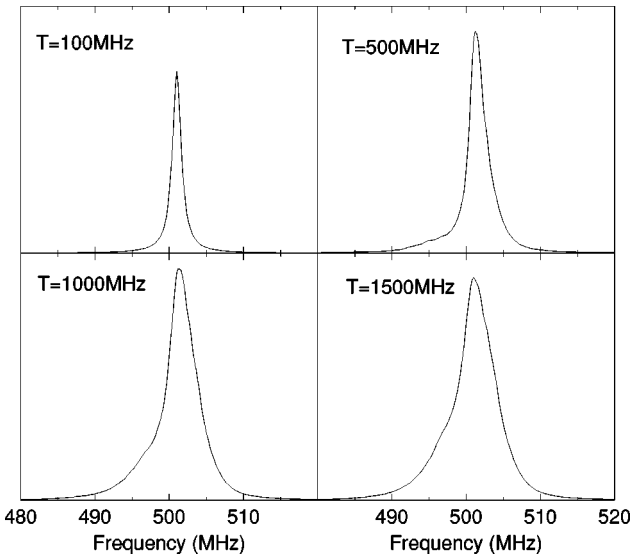

FIG. 7. The exact power spectrum for four spins at different temperatures, including pseudoquadrupolar interactions of 2 MHz and nearest neighbor interactions of 1 MHz. The temperatures ($T = h\nu/k_b$) are 4.8, 24, 48, and 72 mK.

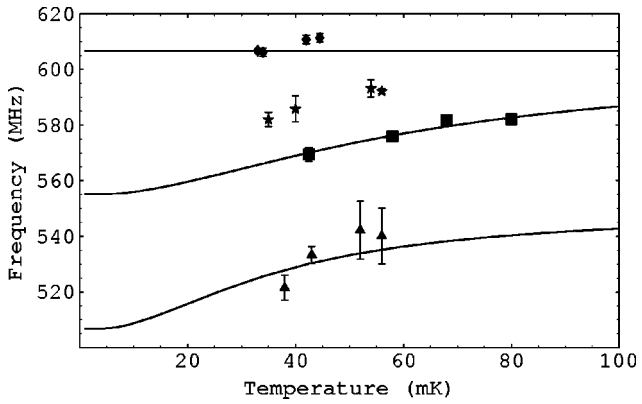

FIG. 8. The theoretical frequencies of the nuclear spin excitations as a function of temperature and the experimental data. The best fit values are $B_A^b = 0.27 \pm 0.03$ T and $B_A^c = 0.81 \pm 0.05$ T.

numerical results also indicate that the lack of line structure in the model is not due to the linearization of the equations of motion.

In order to perform numerical simulations involving more spins, it is simpler to work in a classical system. The classical equations of motion for a Suhl-Nakamura Hamiltonian can be linearized by replacing I_i^z with its thermodynamic average $\langle I^z \rangle$, in all quadratic terms and frequency pulling is predicted. In order to justify this linearization procedure, classical simulations were performed with an array of 15 by 15 nuclear spins with up to third nearest neighbor interactions at a variety of different temperatures. The results agreed well with the classical prediction.

A simulation involving an array of 12 by 12 triplets of spins was also performed. Only interactions within a triplet of spins were included in the calculation. The results qualitatively confirm the quantum mechanical picture as discussed in Sec. III D, and do not show any structure in the resonant lines. Unfortunately, due to numerical limitations, it was not possible to include sufficiently long range interactions to compare the simulations to experimental data. The numerical simulations indicate that the observed line structure cannot be explained as an enhanced pseudoquadrupolar splitting or as a result of the nonlinearity of the equations of motion.

IV. COMPARING THE THEORETICAL MODEL TO THE EXPERIMENTAL RESULTS

The data and models are plotted together in Fig. 8. The data were obtained from spectra such as that shown in Fig. 2, as explained in Sec. II B. The theoretical lines correspond to the excitation modes described in Sec. III D. The best fit lines are, therefore, the eigenvalues of the matrix $G_{k=0}(T)$ that are functions only of the hyperfine coupling constants, the anisotropy fields and the thermodynamic averages $\langle I_1^z \rangle$ and $\langle I_2^z \rangle$. They are fitted to the experimental data using the anisotropy fields B_A^b and B_A^c as free parameters.

A χ^2 fit was first performed only on the lowest frequency line (corresponding essentially to the precession of the Mn1 spins). This is the obvious choice because the resonance corresponding to the Mn2 spins precessing in phase is split into two lines, and it is unclear which should be used in the fitting. A careful consideration of χ^2 shows that only the smaller of the two anisotropy fields can be determined from this fit. This is essentially because the errors on the low frequency line are relatively large. The slope of the line is therefore difficult to extract from the data. What can be determined is the overall magnitude of the frequency pulling effect which depends principally on the smallest of the two anisotropy fields. It is impossible to determine from this model whether the smallest field corresponds to the *b* or the *c* directions. However, we know from the results of Cowen *et al.*[11] that B_A^b is the smaller anisotropy field. Our fit then yields $B_A^b = 0.27 \pm 0.03$ T.

In order to determine the value of B_A^c a χ^2 fit was attempted to both of the frequency pulled lines that could correspond to the precession of the Mn2 spins. The free parameter was B_A^c while B_A^b was fixed at 0.27 T. The lower frequency Mn2 line gives an excellent fit with $B_A^c = 0.81 \pm 0.05$ T, while the higher frequency Mn2 line could not be fitted to any reasonable value of χ^2. The optical mode is not frequency pulled and does not have any dependence on the anisotropy fields.

The conclusion is that the Mn1 resonance, and the lower of the frequency pulled Mn2 resonances are described well by our model, with $B_A^b = 0.27 \pm 0.03$ T and $B_A^c = 0.81 \pm 0.05$ T. The higher of the frequency pulled Mn2 lines is an excitation not described by our model. The relatively small errors are an indication of the sensitivity of the frequency pulling to the anisotropy fields. It is not possible to obtain a reasonable fit of both the Mn1 and Mn2 frequency pulled lines with a model involving only uniaxial anisotropy.

The values of the anisotropy fields previously measured at 1.2 K are $B_A^b = 0.14$ T and $B_A^c = 0.86$ T.[11] While our results for B_A^c are entirely consistent with this result, B_A^b is significantly different. One explanation for this discrepancy is that the anisotropy fields depend on temperature, and were only previously measured at 1.2 K. Our fits provide a value of the anisotropy fields at the zero temperature limit because they are measured at $T < 100$ mK while $T_c \sim 3$ K. Cowen *et al.* showed a trend for B_A^b to increase with decreasing temperature, in agreement with our result, but did not report the behavior of B_A^c. Another explanation is that only quadratic terms in S_i^b and S_i^c were included in the original electronic spin Hamiltonian [Eq. (11)]. In our model it is justified to ignore higher order terms because $\langle S_i^a \rangle \simeq S$, but Cowen *et al.* measured the anisotropy fields by finding the applied magnetic field necessary to force the magnetization into the *b* and *c* directions. In that case, it is not justified to ignore higher order terms, the presence of which could lead to the discrepancy between the two measurements.

Although the resonant lines measured experimentally are shifted downwards in frequency as a function of temperature, and the magnitude of the overall shifts agree well with the theory, there are several places where the model fails. The existence of four observed lines rather than two, the mechanism of absorption above 600 MHz, near the unpulled frequency, and the small temperature dependence of the unpulled frequency is not explained by our model.

The linearization procedure consisting of replacing I_i^z with its thermodynamic average $\langle I^z \rangle$, in the equations of motion and the artificial equivalence of the two Mn2 sites makes it impossible for the optical mode to absorb power from the rf field. In other words, the model introduces too much artificial symmetry into the system and the mechanism of absorption of the unpulled optical mode is lost.

If we do not treat each triplet of electronic spins as a single, $S=5/2$ spin, then we must include 6 atoms per unit cell. Furthermore, there is the possibility of different anisotropy fields for each of the 6 ions. Crystal symmetries prevent different anisotropy fields for the two triplets in each unit cell, but it is likely that the anisotropy fields for the Mn1 sites and the Mn2 sites are different. These details that were neglected in the model will clearly break down many of the symmetries that prevent absorption of optical Mn2 excitation in which, presumably, there will be some admixture of the Mn1 nuclear spin. There could also be a small temperature dependence of this optical line. A full calculation might also predict another excitation mode not presently seen in our model corresponding to the unexplained resonance.

The possibility that some of the observed structure is due to domains was also considered. The magnetic behavior of MnAc at low temperatures has been studied by SQUID magnetometry.[6] At very low fields ($B<14$ mT), there exist mixed phases of ferromagnetic and antiferromagnetic alignment of the *a*-*b* planes, but no domain structure was observed at higher applied fields. In our experiment, we measured the same line structure at applied fields up to 110 mT. (Higher fields were not possible due to the increase in T_1.) It is therefore concluded that domains do not account for the observed structure.

In an effort to explain the fourth resonant line without calculating the electronic spectrum including all six ions per unit cell, we have applied the perturbation technique of Kubo and Tomita,[26] where we regard a single ion Hamiltonian as unperturbed. In this approximation, it is necessary to identify the observed lines in the unperturbed Hamiltonian and the corrections to the positions of the lines can then be calculated. However, we are unable to account for the observed spectra by including the pseudoquadrupolar lines in the unperturbed Hamiltonian. There is no energy scale of the order of 10 MHz in the basic Hamiltonian except the symmetry breaking effect between Mn1 and Mn2. It is difficult, therefore, to account for four lines, separated by more than 10 MHz using this perturbative approach. This conclusion is supported by the quantum and classical numerical simulations.

The MnAc crystal has low symmetry so that the hyperfine coupling constant might have some anisotropy which is also indicated by the relatively strong anisotropy fields. However, we expect the anisotropy to be small since the magnetic moment of Mn^{++} is spin only. The effect of hyperfine anisotropy is that terms in $I_i^+ I_j^+$ and $I_i^- I_j^-$ appear in the effective Hamiltonian. In other words it has the same effect as the anisotropy fields. Since the hyperfine anisotropy should be small, we expect this to lead to small corrections. Demagnetizing effects can also yield $I_i^+ I_j^+$ and $I_i^- I_j^-$ terms, but the demagnetizing factor for the thin, planar shape is small and, in zero magnetic field, the antiferromagnetic coupling between different layers (in the *a*-*b* plane) ensures that no demagnetizing fields are present. Further, we observe no change in structure on applying a sufficiently large magnetic field to make the sample fully magnetic.

The nuclear spin in MnAc is large ($I=5/2$), and it seems reasonable to expect that spin wave calculations using the Holstein-Primakof transformation ($1/I$ expansion) should yield good results at low temperatures. Spin wave theory does indeed agree with our prediction at low temperatures. However, to treat the effect of higher temperatures using spin wave theory, it would be necessary to introduce coupling between the bosons, making the calculation quite difficult. Since the $T=0$ results agree with our predictions, however, we have some confidence that our model is accurate.

V. CONCLUSION

We have measured the frequency pulling effect in MnAc. The temperature dependence of the frequency pulling could not be explained by a simple model assuming uniaxial anisotropy fields and no coupling between Mn1 and Mn2 spins. Furthermore, the experimental data shows a spectrum involving four resonance lines, rather than the expected two.

A model including coupling between all the nuclear spins and nonuniaxial anisotropy was developed. This model agrees well with the magnitude and temperature dependence of the frequency pulling and shows that it is highly sensitive to the strength of the anisotropy fields. Classical and quantum simulations support qualitatively the results of the calculations and a spin wave calculation, accurate at $T=0$, agrees exactly with this model at zero temperature.

The absorption of the unpulled optical mode, and the existence of another resonance mode (presumably mainly involving precession of the Mn2 spins) is likely lost in the approximation that each triplet of electronic spins behaves as a single, $S=5/2$ spin. Although there are too many unknown parameters to make a full calculation worthwhile, it is clear that including the full electronic magnon spectrum will break many of the artificial symmetries that prevent absorption of the unpulled optical line, and the existence of another frequency pulled Mn2 resonance.

We believe, however, that the essential physics of the nuclear magnon excitations has been captured by the model. The model is also of interest in itself because it extends the theory of frequency pulling to cases with $I \geqslant 1/2$ where the self-interaction term is important and to cases where the crystalline anisotropy fields are not uniaxial.

ACKNOWLEDGMENTS

This research was supported by the National Science and Engineering Research Council of Canada. We would like to thank Ian Affleck and Girgl Eska for helpful suggestions.

[1] See, e.g., D. Landau and M. Krech, J. Phys.: Condens. Matter **11**, R179 (1999); T. Nagao and J. Igarashi, J. Phys. Soc. Jpn. **67**, 1029 (1998).
[2] See, e.g., G. Seewald, E. Hagn, and E. Zech, Phys. Rev. Lett. **79**, 2550 (1997); **78**, 5002 (1997); W. D. Hutchinson, M. J. Prandolini, S. J. Harker, D. H. Chaplin, G. J. Bowden, and B. Bleaney, Hyperfine Interact. **20/21**, 215 (1999).
[3] H. Suhl, Phys. Rev. **109**, 606 (1958).
[4] T. Nakamura, Prog. Theor. Phys. **20**, 542 (1958).
[5] E. Turov and M. Petrov, *Nuclear Magnetic Resonance in Ferro and Antiferromagnets* (John Wiley & Sons, New York, 1972), see Chap. 2.
[6] M. Le Gros, A. Kotlicki, and B. G. Turrell, Hyperfine Interact. **108**, 443 (1997).
[7] P. Burlet, Solid State Commun. **14**, 665 (1974).
[8] P. Beauvillain and J. Renard, Physica B & C **86-88B**, 667 (1977).
[9] Y. Okuda, M. Matsuura, and T. Haseda, J. Phys. Soc. Jpn. **44**, 371 (1978).
[10] R. Flippen and S. Friedberg, Phys. Rev. **121**, 1591 (1961).
[11] J. Cowen, G. Johnston, and H. V. Till, J. Chem. Phys. **45**, 644 (1966).
[12] H. Abe and H. Morigaki, *Proceedings of the 1st International Conference on Paramagnetic Resonance*, edited by W. Low (Academic Press, New York, 1963) p. 567.
[13] V. Schmidt and S. Friedberg, Phys. Rev. **188**, 809 (1969).
[14] A. Abragam and M. Pryce, Proc. R. Soc. London, Ser. A **205**, 135 (1951).
[15] See, e.g., *Table of Isotopes*, 8th ed., edited by R. B. Firestone and V. S. Shirley (John Wiley, New York, 1996).
[16] P. De Gennes, P. Pincus, F. Hartmann-Boutron, and J. Winter, Phys. Rev. **129**, 1105 (1963).
[17] See, e.g., K. S. Krane, in *Low Temperature Nuclear Orientation*, edited by N. J. Stone and H. Postma (North-Holland, Amsterdam, 1986), Chap. 2.
[18] A. Kotlicki and B. Turrell, Phys. Rev. Lett. **56**, 773 (1986).
[19] P. Groth, *Chemische Krystallographie* (W. Engelmann, Leipzeg, 1910), Vol. 3, p. 69.
[20] J.-P. Blaizot and G. Ripka, *Quantum Theory of Finite Systems* (MIT Press, Cambridge, 1986), see Chap. 3.
[21] N. Ashcroft and N. Mermin, *Solid State Physics* (Saunders College Publishing, New York, 1976), see Chap. 33.
[22] M. Fisher, Rep. Prog. Phys. **30**, 615 (1967).
[23] S. Vonsovskii, *Ferromagnetic Resonance* (Israel Program for Scientific Translations, Jerusalem, 1964), see Chap. 3.
[24] J. V. Vleck, Phys. Rev. **74**, 1168 (1948).
[25] P. Pincus, Phys. Rev. **131**, 1530 (1963).
[26] R. Kubo and K. Tomita, J. Phys. Soc. Jpn. **9**, 888 (1954).